MnO Nanoparticles Embedded in Functional Polymers as T_1 Contrast Agents for Magnetic Resonance Imaging

Michele Mauri,[1,†] Veronica Collico,[2,†] Lucia Morelli,[2,†] Pradip Das,[2] Isabel García,[3,4] Jesus Penaranda Avila,[2] Michela Bellini,[2] Rany Rotem,[2] Marta Truffi,[5] Fabio Corsi, [5,6] Roberto Simonutti,[1] Luis M. Liz-Marzán,[3,4,7] Miriam Colombo,[2,] Davide Prosperi[2,6]*

[1] Department of Material Science, University of Milano-Bicocca, Via R. Cozzi 55, 20125, Milan, Italy. [2] NanoBioLab, Department of Biotechnology and Biosciences, University of Milano-Bicocca, Piazza della Scienza 2, 20126, Milan, Italy. [3] CIC biomaGUNE, Basque Research and Technology Alliance (BRTA), Paseo de Miramón 182, 20014 Donostia–San Sebastián, Spain. [4] Centro de Investigación Biomédica en Red, Biomateriales, Bioingeniería y Nanomedicina (CIBER-BBN), Paseo de Miramón 182, 20014 Donostia–San Sebastián, Spain. [5] Nanomedicina Laboratory, Department of Biomedical and Clinical Sciences “L. Sacco”, via G. B. Grassi, 74, 20157 Milan, Italy. [6] Breast Unit, Surgery Department, ICS Maugeri IRCCS, via S. Maugeri 10, 27100 Pavia, Italy. [7] Ikerbasque, Basque Foundation for Science, 48013 Bilbao, Spain.

KEYWORDS: Manganese oxide nanoparticles; active polymer coating; magnetic resonance imaging; contrast agents; relaxivity; plasma effect.

ABSTRACT

The design and development of contrast agents (CAs) for magnetic resonance imaging (MRI) in clinical analysis is expected to improve image spatial resolution and to increase detection sensitivity, especially regarding neurological disorders and cancer disease. In particular, advanced CAs for T_1-weighted images are investigated to achieve sensitive detection of early stage primary tumors or brain metastases. In this study, we present a strategy toward diagnostic T_1 contrast agents for MRI, based on polymer-modified MnO nanoparticles. Two different nanosystems were synthesized, consisting of 1) colloidal MnO nanocrystals wrapped by a multidentate amphiphilic polymer, and 2) MnO nanocrystals embedded into PLGA nanoparticles. These nanosystems were compared in terms of their MRI contrast power and biological safety. The latter combines the excellent biocompatibility of PLGA with the unique magnetic properties of MnO nanoparticles and allows sustained contrast enhancement over time. Longitudinal relaxivities of both MnO composite nanomaterials proved to be higher than those of commercial Gd-based contrast agents and Teslascan©, both in phosphate buffer saline and in plasma, also exhibiting low cytotoxicity. The high relaxation rates achieved with these contrast enhancers are promising toward future application in *in vivo* imaging.

INTRODUCTION

Magnetic resonance imaging (MRI) is a non-invasive and efficient medical imaging technique used in daily clinics to visualize the anatomy and physiological processes of patients in real-time.[1] Contrast agents (CAs) are often used in MRI, enhancing image spatial resolution and increasing detection sensitivity.[2] CA efficiency is measured by their longitudinal (r_1) and transverse (r_2) molar

relaxivities, associated to their capability to shorten the spin-lattice (T_1) and spin-spin (T_2) nuclear relaxation times of water protons. CA relaxivity can be tuned by several methods, resulting in the design of a great diversity of agents.[3] Positive CAs (high r_1) are mainly used for neurological examinations and diagnosis of neurodegenerative disorders.[4,5] T_1-weighted images are also expected to allow the direct detection of early primary tumors or brain metastasis.[6] In the clinics, the most frequently used CAs are gadolinium-based probes.[7,8] However, despite their worldwide application, conventional Gd-chelated ion probes exhibit two major limitations: poor sensitivity and, in some cases, long-term accumulation and nephrotoxicity.[9] Although gadolinium remains the gold standard CA in clinical MRI, several cases of nephrogenic systemic fibrosis have been reported in patients treated with Gd CAs[10,11,12,13,14] and, as a result, four Gd-based CAs have been withdrawn from the market in 2017.[15] Such drawbacks reduced the availability of positive CAs, especially if compared with the variety of T_2-based CAs, spawned by the exploitation of superparamagnetic iron oxide nanoparticles[16] or fluorinated copolymers.[17] In this context, manganese ions and their derivatives have been explored as promising alternatives to positive Gd CAs. Mn^{2+} ions have demonstrated a T_1 contrast power comparable to that of Gd(III), increasing the signal intensity of T_1-weighted images.[18] A great advantage of using Mn^{2+} resides in its lower toxicity compared to Gd^{3+} at an equivalent dose.[19] Indeed, manganese is a natural cellular constituent and therefore often found acting as a protein cofactor.[20,21] Hitherto, examples of Mn(II) CAs mainly consist of soluble complexes,[22,23] while only a few Mn CAs based on manganese oxide (MnO) nanomaterials,[242526] metal-organic frameworks[27] and manganese-oxo clusters have been reported.[28,29] Mangafodipir (trisodium Mn(II)-*N,N′*-dipyridoxyl ethylenediamine-*N,N′*-diacetate-5,50-bisphosphate) was the first Mn CA initially approved by the FDA and the EMA, to be commercialized as Teslascan for hepatocyte detection.[30] Unfortunately, Teslascan© was

withdrawn from the market in June 2012 for demonstrated neurotoxicity and commercial reasons,[31,32] thus there are no presently available Mn CAs. The development of molecular formulations is progressing, in particular through the rational synthesis and evaluation of libraries of variant molecules,[33] but a key step forward in expressing the diagnostic potential of Mn CAs is expected by the contribution of nanotechnology. The ability to rationally manipulate nanoparticle (NP) features such as size, shape and surface coating, opens up new opportunities in designing diagnostic nanocarriers to selectively target cells, tissues and metabolic processes.[34,35]

In most studies, MnO particles exhibit very low molar relaxivities, usually in the range 0.2-0.5 mM^{-1} s^{-1}, at least one order of magnitude lower than free Mn^{2+} ions at the same manganese concentration.[36] Such small contrast enhancement in MRI has been attributed to the lack of contact between the core Mn atoms and the surrounding water molecules. Recently, 15-20 nm nanoclusters incorporated inside 140 nm and 1.7 μm poly(lactic-*co*-glycolic acid) (PLGA) particles were reported to strongly enhance the MRI contrast under acidic environment, owing to Mn^{2+} release from the polymer matrix.[37] However, the effectiveness of Mn^{2+} ions is strongly dependent on the interaction with cellular membranes, making the effectiveness of preparations reliant on single Mn ions difficult to validate.[38] On the other side, there is evidence that the interaction of the MnO particle as a whole can be more specifically effective than that of Mn ions: for example, differently shaped particles can display starkly different relaxivities.[39] Also, nanoparticles have the flexibility to be deployed as tunable or activatable systems.[40] Recent work indicates that the relaxivity is extremely sensitive, not only to the particle itself, to the point that it can even be used to distinguish the surface energy of diamagnetic nanoparticles,[41] but also to the coating, since it modulates the interactions between water and the NP surface.[42] In the present work, two different kinds of MnO NPs, based on the same cores but with different polymer coatings, were investigated as safe

positive CAs with improved MRI performance. One system consists of nanoparticles individually coated with the amphiphilic multidentate polymer poly(isobutylene-alt-maleic anhydride), or PMA, which provides an individual coverage to each nanoparticle. The other system comprises multiple particles embedded into large nanoparticles of poly(D,L-lactide–co–glycolide) (PLGA NPs).

EXPERIMENTAL SECTION

Materials. Manganese chloride tetrahydrate ($MnCl_2 \cdot 4H_2O$, 99%), sodium oleate (82%), oleic acid (analytical standard), poly(dl-lactide-*co*-glycolide) (PLGA, MW 24-38 kDa, 50:50), and polyvinyl alcohol (PVA, MW 9-10 kDa, 80% hydrolyzed) were purchased from Sigma-Aldrich (MO, USA). Hexane (97%), chloroform and acetone (99%) were acquired from PanReac AppliChem.

Synthesis of PMA coated manganese oxide nanoparticles (MnO@PMA NPs). The synthesis of oleic acid-coated manganese oxide nanoparticles (MnO NPs) was performed according to a previously reported method.[43] In brief, the metal precursor (manganese oleate) was synthesized *via* overnight refluxing a water-ethanol-hexane solution of manganese (II) salt and sodium oleate. Next, the thermal decomposition of pure manganese oleate in a high boiling solvent, 1-ocadecene, produced high quality hydrophobic MnO NPs.[28,43] The so-prepared MnO NPs were subsequently transferred to an aqueous phase by polymeric coating with poly[isobutene-*alt*-maleic anhydride] reacted in organic solvent with dodecylamine in a 4:3 monomer to dodecylamine molar ratio (PMA).[44]

Synthesis of poly(D,L-lactide–co–glycolide) nanoparticles (PLGA NPs). The carboxyl group-terminated poly(D,L-lactide–*co*–glycolide) (MW 24-38 kDa) nanoparticles (PLGA NPs) were

synthesized by the single emulsion solvent evaporation method.[45] Briefly, 12.5 mg of PLGA dissolved in chloroform (1 mL) was added to an aqueous solution of polyvinyl alcohol (PVA, MW 9-19 kDa, 40 mL, 2% w/w), to form an emulsion under ultrasonic stirring at 40% of amplitude for 30 seconds (twice) in an ice-bath (tip-sonicator Branson, Digital Sonifier). The emulsion was left under magnetic stirring to completely evaporate the organic solvent (4 h). The sample was purified by three-fold centrifugation at 27,237 rcf for 15 min at 4 °C (Scanspeed 173OR, Labogene) and the pellet was re-dispersed twice with PVA solution (0.3 % w/w). Finally, the sample was freeze-dried (Christ, alpha 1-2 LD).

Synthesis of poly(D,L-lactide–*co*–glycolide) coated manganese oxide nanoparticles (MnO@PLGA NPs). The carboxyl group-terminated poly(D,L-lactide–*co*–glycolide) (MW 24-38 kDa) nanoparticles containing MnO NPs (MnO@PLGA NPs) were synthesized through adding 8 mg of MnO NPs to an organic solution of PLGA before ultrasonic stirring under the same experimental conditions. Further steps as mentioned above for the synthesis of PLGA NPs were followed to entrap multiple MnO nanoparticles inside PLGA NPs.

Nanoparticles characterization by DLS and ζ-potential. NP size was characterized by dynamic light scattering (DLS) using a particle size analyzer (90Plus/BI-MAS, Brookhaven Instruments Corp.) operating at 4 mW of a solid-state laser (λ = 633 nm) with a scattering angle of 173º. Measurements were carried out at 25 ºC using a disposable cuvette with 10 mm optical path length. Three measurements per sample were performed to test the repeatability (120 µL, 10 µg mL^{-1} for metal oxide samples and 25 µg mL^{-1} for polymeric samples). Mean hydrodynamic diameters and standard deviations (SD) were calculated with multimodal analysis using Mie theory, by considering the absolute viscosity and the refractive index values of the aqueous medium to be 0.8872 cP and 1.330, respectively. Zeta-potential (ζ) was determined with the same

instrument, equipped with a DTS1070 electrode and data were processed by ZetaPlus Software. ζ-p was automatically calculated from the electrophoretic mobility, based on Smoluchowski theory. A viscosity value of 0.8872 cP, a dielectric constant of 78.5, and Henry function of 1.5 were used for calculations. The mean value from ten measurements gives one record. Analyses were performed in triplicate for each sample (1 mL, 1 μg mL^{-1} for metal oxide samples and 3 μg mL^{-1} for polymeric samples).

Morphological characterization by TEM. NPs morphology was investigated by transmission electron microscopy (FEI Morgagni at 80 kV) and digital images were obtained by means of a CCD Camera System and the Leo Image software. Samples (0.05 μg mL^{-1}) were placed onto a formvar-coated 300 mesh copper grid (Ted Pella, Inc.). The specimen on the copper grid was negatively stained with uranyl acetate (0.2% w/w) only for polymeric samples. Measure IT Olympus Software was used to determine the particle size distribution by measuring about 150 particles (image processing).

Inductively Coupled Plasma–Optical Emission Spectrometry (ICP–OES) analysis. Mn contents were determined by ICP-OES (ICAP 6300, Thermo Fisher Scientific) and an external calibration methodology, after sample degradation in a mixture of 0.75 mL of HCl (36 vol%) and 0.25 mL of HNO_3 (68 % v/v), diluted to 4 mL with Milli-Q water overnight.

Mn^{2+} encapsulation efficiency (%) and loading (μg mg^{-1}). Encapsulation efficiency expresses the amount of metal oxide nanoparticles loaded inside PLGA matrix after NP formulation and was calculated as reported in Eq. 1. Mn^{2+} loading (μg mg^{-1}) is a parameter related to the amount of NPs recovered by ICP analysis after the formulation and the theoretical yield (Eq. 2). ICP analysis were performed by ICP-OES.

Equation (1):

$$encapsulationefficiency(\%) = massof\frac{Mn^{2+}(\mu g)entrapped}{massofMn^{2+}(\mu g)addedreaction} * 100$$

Equation (2):

$$loading(\mu g mg^{-1}) = massof\frac{Mn^{2+}(\mu g)}{massofPLGANPs(mg)}$$

Relaxometric analysis. The magnetic properties of MnO@PLGA NPs and other particles were characterized with a 0.5 T (20 MHz) Time-Domain (TD) NMR benchtop system (Bruker Minispec mq20) with N_2 heating of the sample region. In a typical experiment, 120 µL of NP dispersion was analyzed in 10 mm diameter NMR glass tubes, filling the bottom 8 mm of depth. Standard CPMG (cp_mb) and saturation recovery (sr_mb) sequences were applied to determine the relaxation times T_2 and T_1, respectively. Measurements were performed at 303 K in different media (saline and plasma mixture). Plasma samples were freshly collected from healthy volunteers. In fact, the nanoparticles cannot be prepared directly in plasma, since after preparation they are dispersed in water and cannot be completely lyophilized without altering them. So, diluted stable water dispersion with the maximum possible concentration with plasma, preparing 58.3% v/v solutions. R_1 and R_2 relaxation rates (R) were calculated as $1000/T_1$ or T_2 respectively, while r_1 and r_2 relaxivities (r) coincide with the angular coefficient of the calibration curve R *vs.* concentration, obtained from up to 6 successive dilutions. CPMG experiments were repeated twice on each sample: once before and once after the longer saturation recovery experiment. This scheme ensures the detection of any rapid change in relaxivity, due for example to particle precipitation and aggregation.

In vitro MRI analysis. The magnetic property of MnO@PLGA NPs was characterized by MRI analysis using a 7 T small-bore magnetic resonance scanner equipped with 450/675 mT/m

gradients (slew-rate: 3,400-4,500 T/m/s; rise-time 140 μs) and a mouse body volume-coil (BRUKER, BioSpec 70/30 USR, Paravision 5.1). 500 μL of samples at different concentrations (from 0.003 to 1.0 mM Mn(II) ion concentration) were analyzed at 20.6 °C ± 0.1 °C. RAREVTR (Rapid Acquisition with Relaxation Enhancement (RARE) with variable repetition time) and Multi Slice Multi Echo (MSME) sequences were applied to determine T_1 and T_2, respectively. Measurements were performed at 303 K in saline (0.9% NaCl) or in mixtures of saline and plasma (58.3% v/v). Relaxation rates R and relaxivities were calculated as described above. The software processes the T_1-map and provides the MR images, in which the dynamic contrast is shown as a bright signal.

Cell culture. HeLa cervical cancer cell line was used as *in vitro* cell culture model. Cells were cultured in high glucose Dulbecco's modified Eagle medium (DMEM) supplemented with 10% heat inactivated fetal bovine serum (FBS), 2 mM l-glutamine, 100 U mL^{-1} penicillin, 0.1 mg mL^{-1} streptomycin at 37 °C in a humidified atmosphere containing 5% CO_2. At confluence, the cells were treated using trypsin-EDTA in a 1:4 to 1:6 split ratio, or they were used for experiments. All cell culture materials were supplied by Euroclone S.p.A. (Milano, IT).

MTT assay. In vitro cytotoxicity of MnO@PMA, MnO@PLGA and PLGA NPs was tested on HeLa cells through an MTT assay (CellTiter 96 Non-Radioactive Cell Proliferation Assay, Promega). Cells were seeded in a 96-well plate at a density of 5×10^3 cells per well and incubated for 24 h. Then, cells were incubated with different amounts of the NPs to be tested, six replicates per each concentration. According to the manufacturer's instructions, at the end of the exposure time (24, 48 and 72 h), MTT was added and formazan product was detected after 4 h at 37 °C reading the absorbance at 570 nm with EnSight™ Multimode Plate Reader (Perkin Elmer)

subtracting the absorbance of background at 620 nm. Results were obtained by normalizing the untreated cells set at 100% and expressed as percentage ± SD.

XRD: For X-ray characterization, a D8 Advance powder diffractometer (Bruker) was used with Cu Kα1 radiation (λ =1.5418 Å) and secondary-beam monochromator. The powder is added on a quartz sample holder and measured.

RESULTS AND DISCUSSION

Synthesis and chemical-physical characterization of MnO@PLGA and MnO@PMA NPs. A schematic representation of the preparation of MnO@PLGA and MnO@PMA NPs is illustrated in Scheme 1. In a first setting, a biodegradable PLGA polymer matrix was used to trap and carry MnO NPs, pre-synthesized in organic solvent as MnO nanocrystals stabilized by oleic acid coating, obtaining MnO@PLGA NPs (Scheme 1B). This strategy was aimed at concentrating a large number of MnO NPs inside a nanocarrier that could allow the simultaneous delivery of a sufficient amount of Mn, to cause localized increase in T_1 relaxivity, while decreasing the metal toxicity associated to free ionic Mn^{2+}. The aim of this study was to compare the magnetic properties as T_1 CAs and the biological effects of MnO@PLGA NPs with those of colloidally stable MnO NPs that were obtained by individually wrapping the same paramagnetic MnO nanocrystals into an amphiphilic multidentate polymer poly(isobutylene-alt-maleic anhydride), or PMA, endowed with high affinity for hydrophobic particles (Scheme 1A).

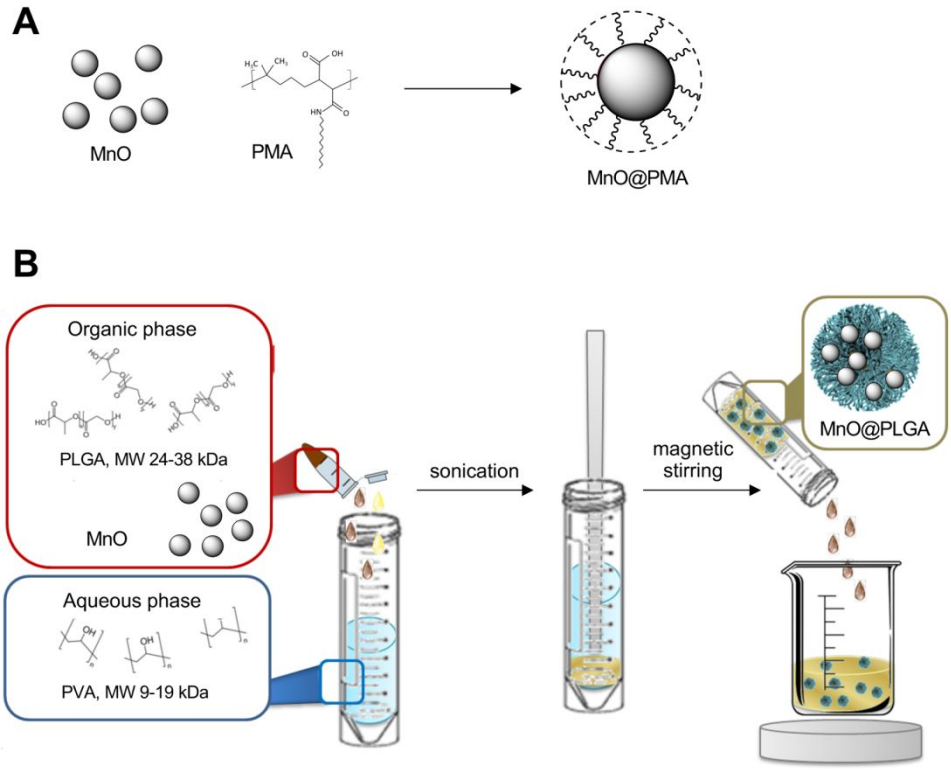

Scheme 1. Schematic representation of the synthesis of a) MnO@PMA and b) MnO@PLGA NPs.

As-synthesized, surfactant-coated MnO nanocrystals[28,43] showed a hydrodynamic diameter of 15.9 ± 0.2 nm in chloroform, as measured by dynamic light scattering (DLS, Fig. 1A), in agreement with transmission electron microscopy (TEM, Fig. 1B), which exhibited homogeneous quasi-spherical NPs of 9.7 ± 1.3 nm. Water-soluble MnO (MnO@PMA) NPs with high colloidal stability were obtained by coating MnO nanocrystals with PMA, synthesized by condensing poly(isobutylene-*alt*-maleic) anhydride with dodecylamine, as previously reported.[44] MnO@PMA NPs exhibited a hydrodynamic diameter of 17.7 ± 0.8 nm (Fig. S1E in the Supplemental Material), and a diffractogram typical of MnO nanocrystals covered with a relatively thick layer of amorphous polymer (Fig. S2).[46] PLGA NPs were prepared by a single emulsion method (see Methods section).[45] To obtain MnO@PLGA NPs, MnO nanocrystals were added to a PLGA (MW 24-38 kDa) solution in chloroform, mixed with an aqueous solution of 2% polyvinyl

alcohol (MW 9-19 kDa), sonicated and freeze dried. Both empty PLGA NPs and MnO@PLGA NPs were colloidally stable in aqueous media and showed comparable sizes (150.5 ± 8.0 nm and 163.0 ± 3.3 nm, respectively, Fig. 1A), with negative surface charge (ζ-potential of –33.5 ± 0.35 mV and –32.1 ± 0.99 mV, respectively). Data from TEM were consistent with DLS size and showed that the NPs maintained their spherical shape after MnO loading (Fig. 1C,D and S1). Figure 1D clearly shows that several MnO nanocrystals were included in each PLGA polymer NP. Notably, the nanocrystals were preferentially located inside the inner core, rather than at the outer shell. Both DLS and TEM size distributions suggest a high degree of monodispersity (Table 1, Fig. 1 and Fig. S1). We thus concluded that the encapsulation of metal oxide nanoparticles did not significantly affect the overall shape, dimension and charge of PLGA NPs.

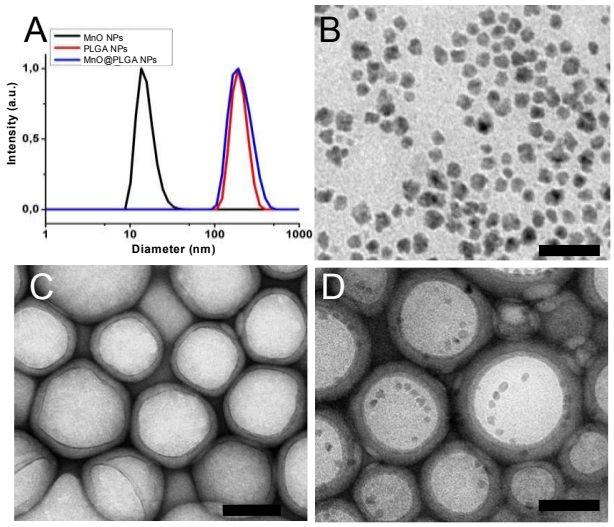

Figure 1. A) Hydrodynamic diameter of MnO, PLGA and MnO@PLGA NPs measured by DLS. B-D) TEM images of (B) MnO (Scale bar = 50 nm), (C) PLGA and (D) MnO@PLGA NPs (Scale bars = 100 nm). Samples were negatively stained with uranyl acetate (0.2% w/w).

Table 1. DLS and ζ-potential data of MnO NPs, PLGA NPs and MnO@PLGA NPs.

	TEM diameter (nm)	DLS diameter (nm)	PDI	ζ (mV)
MnO NPs	9.7 ± 1.3	15.9 ± 0.2	0.130 ± 0.034	—
MnO@PMA	9.7 ± 1.3*	17.7 ± 0.8	0.296 ± 0.22	-40.8 ± 0.70
PLGA NPs	129.5 ± 35.1	150.5 ± 8.0	0.058 ± 0.028	–33.5 ± 0.3
MnO@PLGA NPs	132.8± 41.9	163.0 ± 3.3	0.117 ± 0.013	–32.1 ± 0.99

* same as MnO NPs, PMA not visible at TEM

We assessed the colloidal stability of MnO@PMA and MnO@PLGA NPs in physiological phosphate buffer saline (PBS, pH 7.2) to estimate their potential for biomedical applications. MnO@PMA NPs were highly stable in water and PBS for at least 10 days (Fig. 2A), after an initial swelling from the size values indicated in Table 1 to slightly higher ones, closer to 200 nm. This difference between the first measurable value and the equilibrium value is in line with the smaller diameters measured by TEM, which were performed in vacuum and therefore do not reflect any swelling. MnO@PLGA NPs were first lyophilized for storage, showing a stability of at least 10 days after reconstitution in PBS, according to DLS data (Fig. 2B). An MnO loading of 13.8 ± 2.2 μg per mg of PLGA, corresponding to an encapsulation efficiency (EE%) of 9.65 ± 1.31%, was determined by Inductively Coupled Plasma – Optical Emission Spectrometry (ICP-OES) analysis and proved to be reproducible from batch to batch. For MnO@PMA, a MnO loading of 36 μg per mg of PMA was obtained.

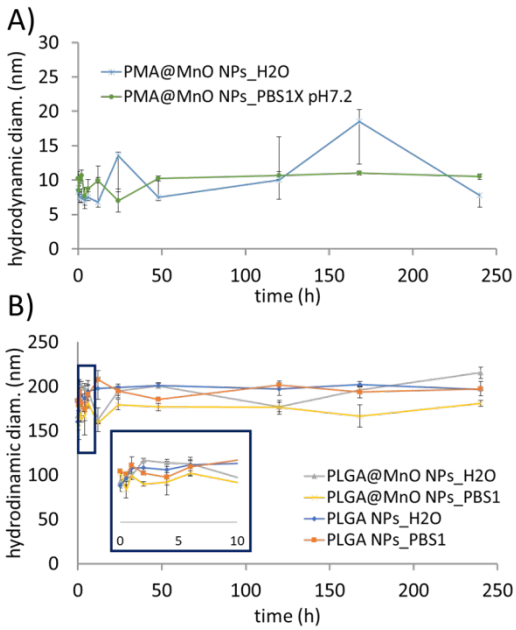

Figure 2. Colloidal stability of (A) MnO@PMA NPs, (B) PLGA NPs and lyophilized MnO@PLGA NPs in water and phosphate buffer solution over 10 days, measured by DLS analysis. The inset shows the evolution during the initial 10 hours.

Relaxometric determination of contrast power of MnO@PLGA and MnO@PMA NPs in aqueous buffer and human plasma. Relaxivity (r) measurements for MnO@PMA and MnO@PLGA NPs were conducted at 310 K, to evaluate the ability of Mn-bearing NPs to reduce the relaxation rates (R) of water protons at 0.5 T, at a temperature close to real biosystems. The longitudinal (T_1) and transverse (T_2) relaxation times of MnO@PMA and MnO@PLGA NPs were first measured in phosphate buffer solution (PBS) with the typical sequences (CPMG and saturation recovery) used for the characterization of magnetic NPs[47]. MnO@PMA NP relaxation rates (R_1 and R_2, calculated as $1/T_1$ and $1/T_2$, respectively, plotted in Fig. 3A) were found to linearly depend on CA concentration, within a wide range (up to the maximum obtainable Mn^{2+} concentration around 0.5 mM), thereby confirming NP stability and absence of aggregation. The longitudinal and transverse relaxivities (r_1 and r_2, determined as the slope in the R *vs*. [Mn^{2+}] plot,

see Fig. 3) in water were estimated to be 7.7 mM^{-1} s^{-1} and 10.5 mM^{-1} s^{-1}, respectively (Fig. 3A). The r_2/r_1 ratio is an important parameter to estimate whether a contrast enhancer can serve as either T_1 or T_2 CA. T_1-agents, such as paramagnetic chelates, usually exhibit r_2/r_1 ratios in a range of 1 to 2.[48] MnO@PMA NPs are thus well suited as T_1 CA, having r_2/r_1 = 1.2 and high r_1 absolute relaxivity values, in line with reportedly excellent NPs.[49] In addition, MnO@PMA NPs maintained constant relaxivity values in water for at least 24 h (Fig S3). Fig. 3B indicates that the linearity of relaxation rate with concentration was maintained for MnO@PLGA in PBS, up to a concentration of 11 mM. Encapsulation of MnO nanocrystals into PLGA as MnO@PLGA NPs increased the solubility, and thus the maximum obtainable concentration of Mn^{2+} in the dispersion increases to 11 mM.

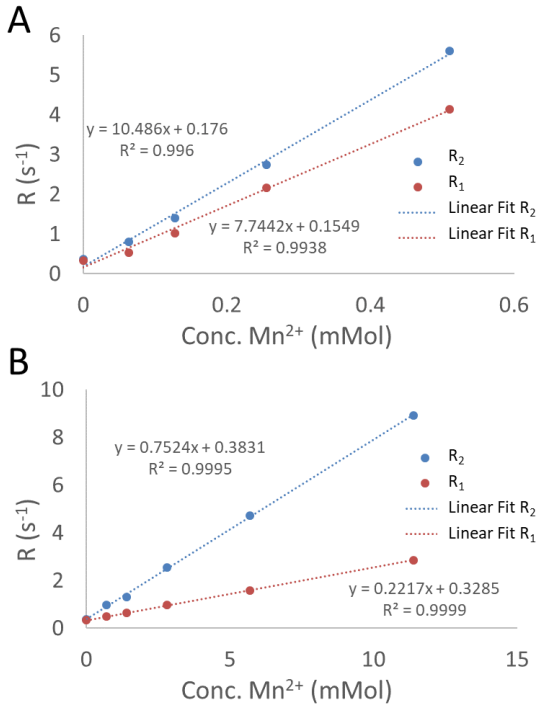

Figure 3. r_1 and r_2 relaxivities calculated from measuring the relaxation rate at different dilutions of A) MnO@PMA in PBS (R_2: y = 10.5x +0.2, R^2 = 0.996; R_1: y = 7.74x + 0.2, R^2 = 0.994; B) MnO@PLGA NPs in PBS (R_2: y = 0.75x + 0.4 R^2 = 0.9995); R_1: y = 0.22x + 0.3, R^2 = 0.9999)

Interestingly, the absolute values of relaxation rates are not much higher than those achievable by PMA coated nanoparticles at lower concentrations, resulting in much smaller values of r_1 and r_2 (r_1: 0.22 mM^{-1} s^{-1}; r_2: 0.75 mM^{-1} s^{-1}; $r_2/r_1 = 3.4$, Fig. 3C). This variation of more than one order of magnitude is due to the presence of the PLGA matrix in MnO@PLGA NPs, which is likely to reduce the CA interaction with water molecules, thereby decreasing the spin-spin and spin-lattice relaxation from the CA to the surrounding medium much more pronouncedly, as compared to the thin PMA layer in MnO@PMA NPs.[50] The detected 3-fold increase of the r_2/r_1 ratio, in comparison to MnO@PMA NPs also points toward a difference in accessibility, since T_2 relaxation is related to longer range effects compared to T_1, and the ratio changes since r_1 was more strongly affected by PLGA encapsulation. Importantly, also MnO@PLGA NPs relaxivities remained constant over 24 h in water (Fig. S3). To evaluate the contrast power of the NPs, their longitudinal relaxivity was then compared with Teslascan© data available in the literature (r_1: 1.85 mM^{-1} s^{-1}; r_2: 2.18 mM^{-1} s^{-1}; r_2/r_1 = 1.2).[51] The relaxation of MnO@PMA was found to be even higher than that reported for Teslascan©, suggesting a superior efficacy for MnO@PMA NPs as a contrast enhancer *in vitro*, compared to commercial CAs. Note that this is an improvement also over many Mn systems presented in literature, that mostly present lower absolute r_1 values,[26] or very high r_2/r_1 ratios.[27] In contrast, the relaxation of MnO@PLGA NPs was 2.7 times lower than that of Teslascan©. However, in order to fully appreciate the potential of these composite NPs for future *in vivo* MRI applications, relaxation times for both MnO@PMA and MnO@PLGA NPs were further analyzed in human plasma (Figs. 4 and 5). For the experiments in Fig, 4, we prepared solutions with different amounts of MnO particles, selected to start with roughly the same absolute R_1.

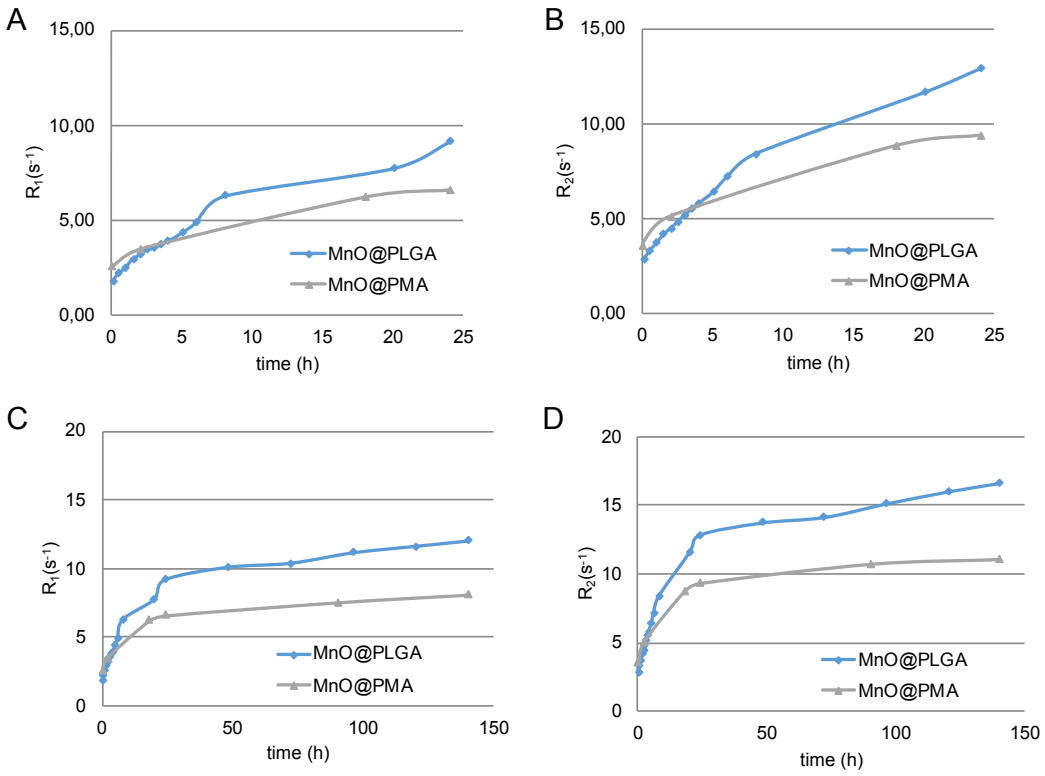

Figure 4. R_1 and R_2 of MnO@PLGA and MnO@PMA NPs (120 µL, 917 µg mL^{-1} MnO@PLGA NPs. 88 µg mL^{-1} MnO@PLGA) relaxation rates in plasma from three different donors for 24 h (A and B, respectively) and for 6 days (C and D, respectively).

In plasma, MnO@PMA r_1 and r_2 increased immediately after dispersion to 14.5 mM^{-1} s^{-1} and 16 mM^{-1} s^{-1}, respectively, whereas the r_2/r_1 ratio remained near 1.1. For MnO@PLGA, relaxivities measured immediately after sample preparation were 0.68 m^{-1} s^{-1} (r_1) and 0.71 mM^{-1} s^{-1} (r_2) (Fig. 3S B,C). This also brought the ratio close to 1, indicating a different mechanism of interaction, which is to be expected since the interaction between the NPs embedded in the PLGA coating and water is mediated by PLGA itself, which is sensitive to the presence of various plasma molecules. Still, the absolute values were low, as observed when assessing Gd response in plasma, where gadolinium forms complexes with blood proteins which partially mask the paramagnetic effect.[19]

Both MnO@PMA and MnO@PLGA NPs showed kinetic profiles in plasma that were significantly different from those measured in PBS (Fig. 4). In plasma, we observed a burst increase in both R_1 and R_2 within the first 6 h, followed by a change in slope leading to a milder increase during the subsequent 24 h. This experiment was extended for 120 h, confirming the trend.

Since the effect appeared much more pronounced in MnO@PLGA, with an increase of one order of magnitude, we replotted the data from plasma and PBS in Fig. 5, also reporting the r_2. The wide error bars present in the figure indicate a high sensitivity to the specific composition of the plasma from different donors. Still, the kinetic profile was consistently the same, with both relaxation values surpassing those of Teslascan© over time. This confirms that the increased relaxation properties are inherent to the evolution of the material and independent from inhomogeneities of the environment composition. An estimate of r_1 and r_2, based on the ratio between maximum R values and concentration, yielded 11.38 mM^{-1} s^{-1} for r_2 and 8.26 mM^{-1} s^{-1} for r_1. We assumed that the increase of R_1 and R_2 over time was due to a release of either Mn^{2+} ions or MnO NPs from the carriers, resulting in a more effective interaction with the surrounding medium. The values estimated above also produced an r_2/r_1 ratio of 1.38, indicating that the most relevant mechanism is the interaction of NPs with water.

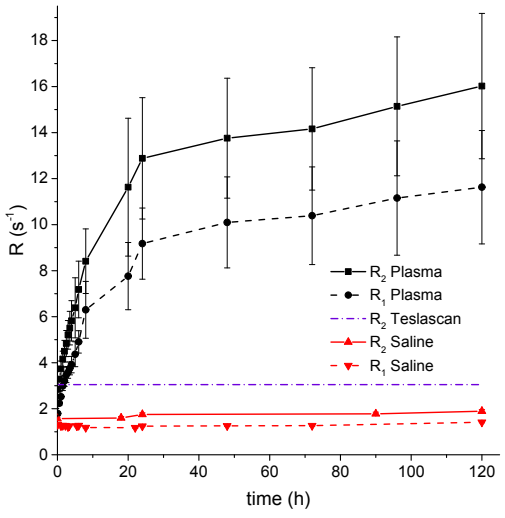

Figure 5. R_1 and R_2 values for MnO@PLGA in PBS and in plasma, up to 120 h. Both samples contained 100 mg mL^{-1} of CA, corresponding to 1.4 mmol of Mn^{2+}. The dashed line represents the expected R_2 relaxivity for the same amount of Teslascan©. The values presented for plasma are an average from three experiments performed with plasma from different donors. SDs for measurements conducted in PBS were <1%.

The phenomena discussed above are summarized in Table 2, where both the high intrinsic efficiency of MnO@PMA NPs and the peculiar behavior of MnO@PLGA in plasma clearly stand out.

Table 2. Summary of r_1 and r_2 values of the novel NPs and the Teslascan© benchmark. Relaxivities are expressed in mM^{-1} s^{-1}. Values in italic are not rigorously obtained as a slope, but rather estimated using a single point at a known concentration. Standard deviations omitted for clarity are less than 4% except for MnO@PLGA, where differences between plasma donors increase the variability.

Sample	**r_1**	**r_2**	**r_2/r_1**	**Time Evolution r_1**
In PBS				
MnO@PMA	7.7	10.4	1.35	Stable
MnO@PLGA	0.24	0.82	3.4	Stable
Teslascan©	1.85	2.18	1.2	Stable
In Plasma				
MnO@PMA	*14.5*	*16.0*	1.1	Increase to 31±1
MnO@PLGA	*0.68*	*0.71*	1.05	Increase to *8.3±1.5*

Possible mechanisms for the latter effect include the swelling of the polymeric matrix or the faster degradation of PLGA polymer in plasma compared to PBS. Indeed, released MnO NPs were expected to produce also a progressive and sustained release of Mn^{2+} ions, with a concomitant increase in T_1-weighed MR signal. It is likely that the small aqueous CAs exhibited higher relaxation rates by reducing molecular motion due to interactions with serum proteins.[5253] In support to this interpretation, we observed that Mn^{2+} ions in plasma led to greater T_1 shortening as compared to PBS, in a wide concentration range (Table 3). On the other hand, the ions produced by dissolution of $MnCl_2$ did also produce a very high r_2/r_1 ratio, around 10 in PBS and 5 in plasma, supporting the hypothesis of the relaxation being due to the whole NPs. On itself, T_1 reduction can be attributed also to ions,[38] but low r_2/r_1 is typical of whole NPs. Compared to the literature,[37] it is important to note that we used PLGA with low molecular weight: it is commonplace for the MW of a polymer coating to regulate its mobility and entanglement, and thus the access to its surface.[54]

Table 3. R_1 and R_2 values of $MnCl_2$ solutions in PBS (pH 7.4, 100 mM) and plasma (4 h of incubation) measured at 37 °C and in a Time-Domain NMR spectrometer working at clinical MRI field (1.5 T). Error always below 1%. From the values, r was also calculated and reported in the table.

conc Mn^{2+} (mM)	**R_1 in PBS (ms)**	**R_1 in plasma (ms)**	**R_2 in PBS (ms)**	**R_2 in plasma (ms)**
0.25	1.5	10.4	19.7	23.1
1	5.5	20.7	66.3	56.9
10	50.9	105.2	609.8	530.2
r ($mMol^{-1}$ s^{-1})	5.06	9.58	60.47	52.26

Phantom analysis of contrast enhancement using MnO@PLGA NPs by MRI. Longitudinal relaxation times of polymeric NPs were measured by an MR scanner at 7 T to preliminarily investigate the MRI positive contrast power. The T_1-weighed images showed a clear dose-dependent signal in both PBS and plasma (Fig. 6A,B), in agreement with time-domain NMR (TD-NMR) data. The r_1 of NPs remained constant in PBS, while it increased over time in plasma. MRI analysis thus confirmed TD-NMR data. No contrast was detected in both physiological media and in plasma for control PLGA NPs (data not shown).

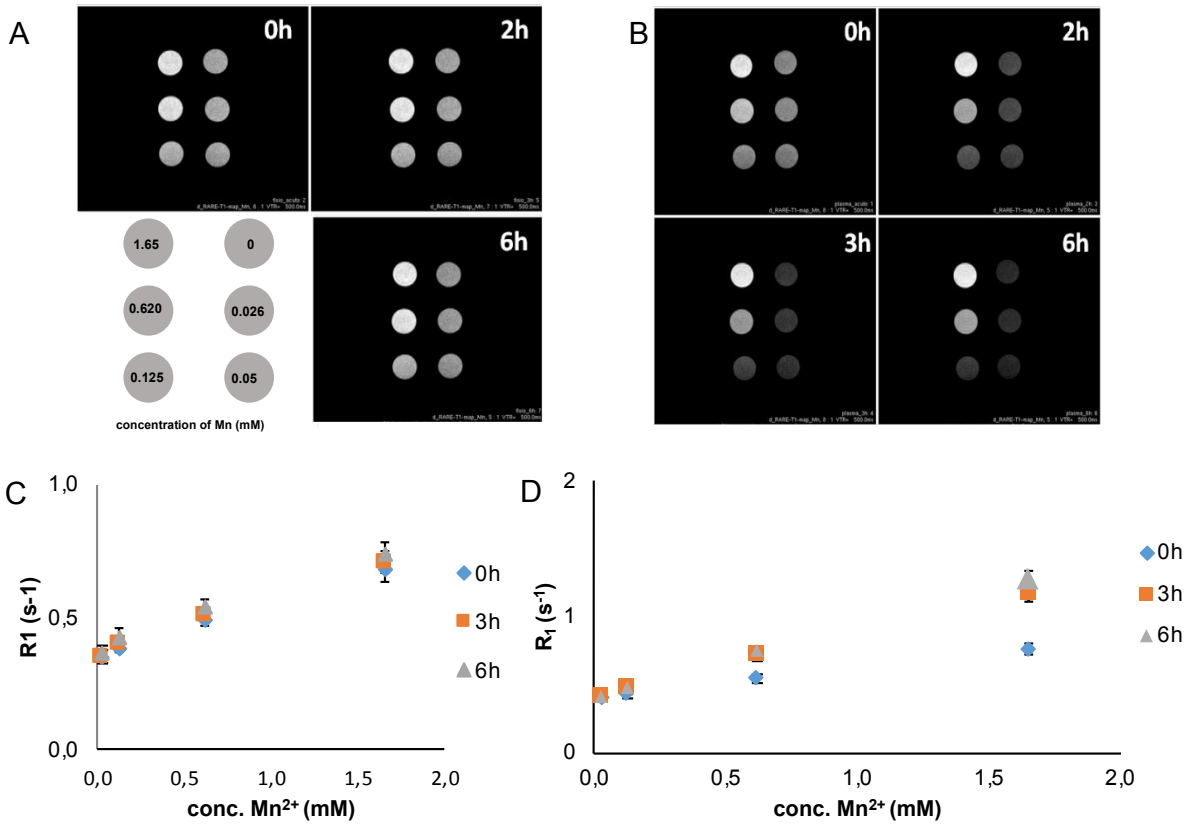

Figure 6. T_1-weighted images of MnO@PLGA NPs at different concentrations of Mn^{2+} ions (in the range 0-1.65 mM) in (A) PBS and (B) plasma; R_1 of MnO@PLGA NPs in (C) PBS and (D) plasma as a function of Mn^{2+} concentration (0-1.65 mM) and time (0-6 h).

Relaxation rates as a function of Mn^{2+} ion concentration (Fig. 6C,D and S4) clearly demonstrated that the values of r_1 remained stable in PBS for at least 6 h (0.201 ± 0.008 mM^{-1} s^{-1}). As expected from TD-NMR and MRI studies, the relaxivity of MnO@PLGA NPs increased over time at all tested concentrations, in the presence of plasma (r_1 raised from 0.217 to 0.532 mM^{-1} s^{-1}). In particular, it was observed that the initial r_1 in plasma matched the r_1 values in PBS. This observation confirmed that no sample degradation occurred within minutes after MnO@PLGA NPs dispersion in plasma. To check whether the effect of entire nanoparticles or Mn^{2+} ions was prevalent either in PBS or plasma, we measured the release of Mn^{2+} ions in both media. As indicated in Fig. S5, the particles were partly dissolved, but only after several hours and never completely. These data support the opsonisation hypothesis, according to which the time-dependent r_1 enhancement was caused by the release of MnO CA from PLGA NPs in plasma, most likely due to matrix swelling rather than to polymer degradation. From MRI data of MnO@PLGA NPs, 0.026 mM Mn^{2+} was the minimum concentration that could provide a detectable signal.

Investigation of cytotoxicity profile for MnO@PLGA and MnO@PMA NPs. The toxicity of Mn-based CAs is primarily due to the action of Mn^{2+} as a calcium channel blocker with effects on muscle electrophysiology and contractility. This effect has limited the use of Mn^{2+} salts as paramagnetic CAs for *in vivo* diagnosis.[5556] In addition, Mn^{2+} complexes are relatively unstable *in vivo* and tend to dissociate in biological media. Indeed, Mn ions can be displaced by other divalent cations, such as Ca^{2+}, Mg^{2+}, or Zn^{2+}. Hence, some concerns exist about the potential long-term toxicity associated with the use of Mn CAs.[575859] Therefore, to assess the potential of MnO@PMA and MnO@PLGA NPs as CAs, we investigated their toxicity *in vitro*. Cytotoxicity tests using representative HeLa cancer cells demonstrated that both PLGA NPs and MnO@PLGA NPs were safe in the tested concentration range (Fig. 7). The low toxicity of the NPs was confirmed by ROS

assay (Fig. S6): the amount of ROS, detected after 24h, did not induce any toxic effect, as demonstrated by MTT analysis. Table 4 correlates PLGA weight and Mn^{2+} concentration. After 72 h of incubation, the viability of treated cells was comparable to that of the control. In contrast, MnO@PMA exhibited mild time- and dose-dependent cytotoxicity above 15 nM (Fig. 7), suggesting that the cytotoxicity observed using MnO@PMA NPs was prevented by PLGA coating.

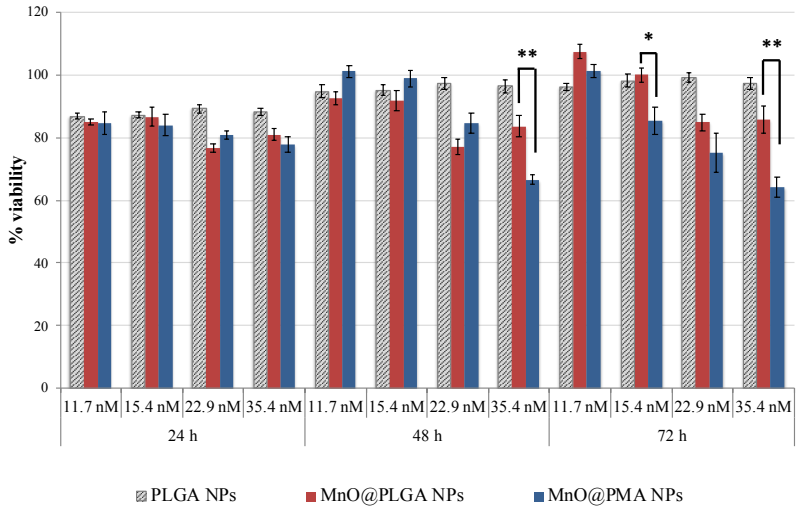

Figure 7. *In vitro* cytotoxicity study in HeLa cells. Cell viability was assessed by MTT assay. Cells treated for 72 h with PLGA NPs; MnO@PLGA NPs; and MnO@PMA NPs. Reported values are the mean of five replicates ± s.e. normalized on the proliferation of untreated cells. *P <0.05; **P <0.01 (Student's *t*-test).

Table 4. Mn ions concentration relative to nanoparticles dosages used in bioavailability experiments.

[PLGA NPs] (mg mL^{-1})	**[MnO NPs](μg mL^{-1})**	**[Mn(II)] (μg mL^{-1})**	**[Mn(II)] (nM)**
0.05	3.9	0.6	11.7
0.06	4.9	0.8	15.4

0.49	45.4	1.3	22.9
0.98	91.7	1.9	35.4

CONCLUSIONS

In summary, two Mn-based nanoprobes were investigated as safer and effective positive contrast enhancers, with the objective of providing alternatives to Gd and Teslascan©. MnO@PMA NPs showed higher longitudinal relaxivity compared to Gd-based CAs and Teslascan©,[60] while maintaining a low r_2/r_1 ratio, both in PBS and plasma, also exhibiting low cytotoxicity. An improved biodegradable Mn-based nanocomposite, consisting of MnO nanoclusters incorporated into PLGA NPs (MnO@PLGA) was synthesized. MnO@PLGA NPs offered the advantage of lower toxicity with 3-fold higher T_1-contrast power compared to Gd and Teslascan©. Our water-soluble MnO@PLGA CAs exhibited a very pronounced dose- and time-dependent r_1 increase in plasma, possibly due to the use of relatively short PLGA as compared to the literature, thereby favoring the release of active NPs in plasma while maintaining a high particle stability in PBS. Comparison with relaxation phenomena induced by Mn ions in the same solutions, which are characterized by ratios close to 10 and thus very far from the ideal value of 1, indicate that the measured properties are the unique result of the release of entire nanoparticles. This unforeseen property is particularly attractive in view of clinical translation: the localized release of contrast agent at target cells or tissues by either passive (*i.e.*, via the enhanced permeability and retention effect) or active (*i.e.*, exploiting NP functionalization with selective ligands) targeting offers the chance to strongly improve the signal intensity over time, further enhancing MRI sensitivity. The use of these CAs brings new challenges for clinical application. Commercially available CAs are non-specific, whereas PLGA and PMA polymers have been proposed as basic envelopes, suitable

for subsequent surface bioengineering with selective ligands (*e.g.*, small molecules, peptides and antibodies) for molecular recognition associated to specific disorders. In addition, therapeutic agents or secondary imaging components can be loaded into PLGA nanoparticles, resulting in multifunctional theranostics for early detection, diagnosis, and personalized treatments. The combination of all these properties makes MnO@PMA and MnO@PLGA NPs promising nanoprobes for molecular imaging.

ASSOCIATED CONTENT

Supporting Information. TEM images, DLS size distribution of NPs (Fig. S1), XRD diffractogram of MnO@PMA NPs (Fig. S2), R_1 and R_2 stability of NPs (Fig. S3), release profile of Mn^{2+} (Fig S4) and T_1-weighted images of different concentrations of MnO@PLGA NPs (Fig. S5). This file (PDF) is available free of charge.

AUTHOR INFORMATION

Corresponding Author

* Dr. Miriam Colombo, Università degli Studi di Milano-Bicocca, Dipartimento di Biotecnologie e Bioscienze, Piazza della Scienza, 2 - 20126 Milan, Italy. Phone: +39 02 6448 3388; Email: miriam.colombo@unimib.it

Author Contributions

The manuscript was written through contributions of all authors. All authors have given approval to the final version of the manuscript. †These authors contributed equally to this work.

Funding Sources

Financial support from the Italian Ministry of University and Research (MIUR) through grant "Dipartimenti di Eccellenza-2017" to University of Milano Bicocca, Department of Biotechnology and Biosciences, and Spanish Ministerio de Ciencia e Innovación (Grant No. MAT2017-86659-R) are acknowledged.

Notes

The authors declare that they have no competing interests.

ACKNOWLEDGMENT

We thank T. Canu and A. Esposito (IRCCS San Raffaele Hospital, Milano) for Magnetic Resonance service. We thank Silvia Ferrario (Graftonica) for performing XRD.

ABBREVIATIONS

CA, contrast agent; NP, nanoparticle; MRI, magnetic resonance imaging; PLGA, poly(lactic-*co*-glycolic) acid; r_1, longitudinal relaxivity; r_2, transverse relaxivity; T_1, spin-lattice relaxation time; T_2, spin-spin relaxation time; R_1, longitudinal relaxation rate; R_2, transverse relaxation rate; PMA, poly[isobutene-*alt*-maleic anhydride] graft dodecylamine (75%) polymer; ICP-OES, Inductively Coupled Plasma Optical Emission Spectrometry; TD NMR, time-domain nuclear magnetic resonance; TEM, transmission electron microscopy; DLS, dynamic light scattering; PBS, phosphate buffer saline; PDI, polydispersity index; ξ, zeta-potential;

REFERENCES